



Published in final edited form as:

JCI Insight. 2016 ; 1(2): e85817-. doi:10.1172/jci.insight.85817.

Heme oxygenase-1 regulates mitochondrial quality control in the heart

Travis D. Hull^{1,2}, Ravindra Boddu^{1,3}, Lingling Guo^{2,3}, Cornelia C. Tisher^{1,3}, Amie M. Traylor^{1,3}, Bindiya Patel^{1,4}, Reny Joseph^{1,3}, Sumanth D. Prabhu^{1,4,5}, Hagir B. Suliman⁶, Claude A. Piantadosi⁷, Anupam Agarwal^{1,3,5}, and James F. George^{2,3,4}

¹Department of Medicine, University of Alabama at Birmingham, Birmingham, Alabama, USA

²Department of Surgery, University of Alabama at Birmingham, Birmingham, Alabama, USA

³Nephrology Research and Training Center, University of Alabama at Birmingham, Birmingham, Alabama, USA

⁴Comprehensive Cardiovascular Center, University of Alabama at Birmingham, Birmingham, Alabama, USA

⁵Department of Veterans Affairs, Birmingham, Alabama, USA

⁶Department of Anesthesiology, Duke University School of Medicine, Durham, North Carolina, USA

⁷Department of Pulmonary, Allergy and Critical Care, Duke University School of Medicine, Durham, North Carolina, USA

Abstract

The cardioprotective inducible enzyme heme oxygenase-1 (HO-1) degrades prooxidant heme into equimolar quantities of carbon monoxide, biliverdin, and iron. We hypothesized that HO-1 mediates cardiac protection, at least in part, by regulating mitochondrial quality control. We treated WT and HO-1 transgenic mice with the known mitochondrial toxin, doxorubicin (DOX). Relative to WT mice, mice globally overexpressing human HO-1 were protected from DOX-induced dilated cardiomyopathy, cardiac cytoarchitectural derangement, and infiltration of CD11b + mononuclear phagocytes. Cardiac-specific overexpression of HO-1 ameliorated DOX-mediated dilation of the sarcoplasmic reticulum as well as mitochondrial disorganization in the form of mitochondrial fragmentation and increased numbers of damaged mitochondria in autophagic

Address correspondence to: James F. George, Division of Cardiothoracic Surgery, Department of Surgery, Rm 790 LHRB, 1720 2nd Ave. South, University of Alabama at Birmingham, Birmingham, Alabama 35294, USA. Phone: 205.934.4261; jgeorge@uab.edu. Or to: Anupam Agarwal, Division of Nephrology, Department of Medicine, Rm 647 THT, 1720 2nd Ave South, University of Alabama at Birmingham, Birmingham, Alabama 35294, USA. Phone: 205.996.6670; agarwal@uab.edu.

Conflict of interest: The authors have declared that no conflict of interest exists.

Author contributions

TDH wrote sections of the manuscript and performed the in vivo studies, Western blots, and coordinated the day-to-day activities of the study. RB performed some of the Western blots and assisted with in vivo studies. LG performed tail vein injections and all surgical procedures. CCT performed the quantitative measurements of the TEM data. AMT coordinated logistics, lab management, and assisted with Western blotting. BP was instrumental in performing the echo measurements. RJ was involved in breeding the animals and genetic screening and generated the relevant mouse strains. SDP made the *cs*-HO-1 mice available and was instrumental in the interpretation of the echo data. HBS and CAP performed measurements of mitochondrial biogenesis. AA and JFG were the principal investigators who provided overall direction of the study, data interpretation, and writing of the manuscript.

vacuoles. HO-1 overexpression promotes mitochondrial biogenesis by upregulating protein expression of NRF1, PGC1 α , and TFAM, which was inhibited in WT animals treated with DOX. Concomitantly, HO-1 overexpression inhibited the upregulation of the mitochondrial fission mediator Fis1 and resulted in increased expression of the fusion mediators, Mfn1 and Mfn2. It also prevented dynamic changes in the levels of key mediators of the mitophagy pathway, PINK1 and parkin. Therefore, these findings suggest that HO-1 has a novel role in protecting the heart from oxidative injury by regulating mitochondrial quality control.

Introduction

Heme oxygenase-1 (HO-1) is an inducible stress response gene that is upregulated as a protective mechanism in disease states of the heart and other organ systems (1–4). HO-1 activity results in the degradation of heme, a prooxidant molecule that increases in bioavailability secondary to cell death from tissue injury (5–7). HO-1 catalyzes the formation of equimolar quantities of carbon monoxide (CO), biliverdin, and iron (Fe²⁺) from heme (6, 8, 9). Biliverdin is immediately converted into bilirubin by biliverdin reductase, while iron is oxidized (to Fe³⁺) and sequestered by ferritin. The protective properties of HO-1 expression can be attributed to both the degradation of heme as well as the production of these cytoprotective byproducts, which possess antioxidant, antiinflammatory, and antiapoptotic properties (10–14).

Mitochondria are dynamic organelles that are exquisitely sensitive to damage from oxidative stress (15). In the heart, they form organized and interconnecting networks through the process of mitochondrial fusion that is mediated by the proteins mitofusin 1 (Mfn1) and Mfn2, which are GTPases located on the outer mitochondrial membrane (16). The process of mitochondrial fusion is balanced with mitochondrial fission, which is mediated in part by the cytosolic protein dynamin-related protein 1 (DRP1) and its partner protein, mitochondrial fission 1 (Fis1) (17–19). Abnormal or depolarized mitochondria, which are potent sources for ROS generation (20, 21), undergo fission and are cleared from cells through the process of mitophagy (15, 22, 23). Ultimately, it appears that tight regulation of mitochondrial dynamics (i.e., fission and fusion) in the healthy heart and in response to cardiac injury is important in maintaining adequate mitochondrial quality control. How mitochondrial dynamics are affected by HO-1 expression in cardiac myocytes is poorly understood.

Macroautophagy is a genetically encoded catabolic process whereby senescent or damaged cellular proteins and organelles are degraded in the autophagosome after fusion with a lysosome. The process of mitochondrial autophagy is referred to as mitophagy, because it is the specific pathway by which senescent or damaged mitochondria are recycled by lysosomal degradation (15). Unique mediators of mitophagy include the effector proteins PTEN-induced putative kinase 1 (PINK1) and parkin. PINK1 binds to depolarized mitochondria and recruits the E3 ubiquitin ligase, parkin (24–29), thus marking mitochondria for mitophagy through ubiquitination. As damaged mitochondria are cleared from the cell, new mitochondria are generated in a process termed mitochondrial biogenesis (30). Biogenesis is a tightly controlled process that is regulated by nuclear transcription

factors, such as nuclear respiratory factor 1 (NRF1) and its coactivator peroxisome proliferator-activated receptor γ coactivator 1 (PGC1 α), which upregulates expression of the mitochondrial transcription factor A (TFAM), thus enabling replication of the mitochondrial DNA (mtDNA) (31–35). Interestingly, oxidative stress, such as that which is caused by DOX, has been shown to activate HO-1 expression as well as the processes of mitochondrial biogenesis and mitophagy through a shared signaling pathway, involving nuclear translocation of NRF2 and binding to antioxidant response elements in the nuclear DNA (36–39). Thus, fission/fusion, mitophagy, and biogenesis converge to constitute the process of mitochondrial quality control (15, 40). Numerous disease states are caused by or result in derangements in mitochondrial quality control. The interplay between HO-1 expression and the global processes that constitute mitochondrial quality control, which include mitochondrial dynamics (fission/fusion), biogenesis, and mitophagy, has not been completely described.

Here, we have validated a model of cardiac mitochondrial dysfunction using the anthracycline doxorubicin (DOX). DOX administration results in significant cardiac dysfunction, as exemplified by reduced ejection fraction, thinning of the left ventricular wall, and dilation of the left ventricular chamber. HO-1 overexpression was protective against DOX-induced dilated cardiomyopathy. At the subcellular level, HO-1 overexpression prevented myofibril disorganization and mitochondrial fragmentation. This protective effect of HO-1 prevented mtDNA depletion and was associated with increased mitochondrial biogenesis. In addition, HO-1 expression abrogated increased expression of the fission-related protein Fis1 and increased the expression of the fusion mediators Mfn1 and Mfn2. It appears that the protective effects of HO-1 expression at the level of the mitochondria resulted in maintenance of the mitophagy pathway at homeostatic levels as opposed to the dynamic changes that occurred with respect to time in WT mice treated with DOX. Thus, HO-1 expression appears to have a generally protective effect on mitochondrial quality control by influencing the processes of biogenesis, dynamics, and mitophagy.

Results

HO-1 overexpression prevents DOX-induced systolic dysfunction and dilated cardiomyopathy

DOX causes myocardial dysfunction through a variety of mechanisms, one of which is dysregulation of mitochondrial homeostasis (41). Therefore, we established a model to study the role of HO-1 in regulating mitochondrial quality control by treating mice with 3 doses of DOX at 6 mg/kg body weight every third day for 1 week (Figure 1A). To test the effect of HO-1 in this system, we compared the results of DOX administration in WT mice to those in mice that overexpress human HO-1 from a bacterial artificial chromosome (BAC) encoding the complete human HO-1 gene and its associated promoter elements (42) (HBAC mice; see Table 1 for a description of the mouse strains used). Western blot analysis of HO-1 protein expression in cardiac left ventricular (LV) muscle confirmed that the BAC transgene results in overexpression of HO-1 in cardiac tissues (Figure 1B). This overexpression was protective against the toxic effects of DOX. The ejection fraction (EF) declined in DOX-treated WT mice over a 14-day period following the final dose of DOX. No such decline was

observed in HBAC mice (Figure 1C). At 14 days after treatment, the mean EF in WT mice was $51\% \pm 5\%$ versus $69\% \pm 1\%$ in HBAC mice ($n = 5-8$, $P = 0.02$). The echocardiographic measurements of LV wall thickness in systole and diastole indicated that DOX treatment induced significant thinning of the wall of the LV in WT mice, which was prevented by HO-1 overexpression in HBAC mice ($P < 0.05$, $n = 5-8$, Table 2). These findings, combined with data showing that the mean diameters of the LV in diastole and systole were significantly larger in WT mice at 14 days after treatment than in the treated HBAC mice (Figure 1, D and E, and Table 2) when compared to baseline values, indicated that DOX treatment causes dilated cardiomyopathy, which is prevented by the overexpression of HO-1.

HO-1 overexpression protects the heart from DOX-mediated damage

Histological analysis confirmed the protective role of HO-1 expression in preventing DOX-induced dilated cardiomyopathy (Figure 2, A and B). In addition, high-magnification microscopy demonstrated that DOX causes cardiomyocyte vacuolization (Figure 2C), hypereosinophilia (Figure 2E), and interstitial edema (Figure 2E). None of these abnormalities were observed in the hearts of treated HBAC mice (Figure 2, D and F). Trichrome staining showed evidence of fibrosis in WT mice treated with DOX (Figure 2, G and H), and flow cytometry showed that the proportion of mononuclear phagocytes ($CD45^+CD11b^+Gr-1^-MHCII^+$) among $CD45^+$ cells in the heart was increased relative to untreated mice and HBAC mice treated with DOX (Figure 2I). These data suggest that DOX treatment results in cardiomyopathy secondary to gross changes in myocardial morphology and that these effects are mitigated by the overexpression of HO-1.

HO-1 expression promotes mitochondrial biogenesis

DOX is toxic to mitochondria (43, 44). Therefore, mice with cardiomyocyte-specific overexpression of HO-1 (*cs*-HO-1) were utilized to assess the role of myocyte HO-1 overexpression on mitochondrial function after DOX treatment (Figure 3A and Supplemental Figure 1; supplemental material available online with this article; doi:10.1172/jci.insight.85817DS1). There was a significant reduction in mtDNA copies in WT mice treated with DOX compared to vehicle-treated controls (Figure 3B), thus supporting previous evidence that DOX is a mitochondrial toxin and suggesting an inability of WT mice to upregulate mitochondrial biogenesis after DOX. mtDNA depletion was prevented in *cs*-HO-1 mice (Figure 3B). HO-1 overexpression also led to increased expression of the mtDNA polymerase, Pol γ , suggesting that HO-1 overexpression promotes the generation of new mitochondria through biogenesis after toxic insult (Figure 3C). Expression of key components of the mitochondrial electron transport chain, NADH dehydrogenase 1 (ND1) (Figure 3D) and cytochrome c oxidase III (COX3) (Figure 3E), was also elevated in *cs*-HO-1 mice but not WT mice after DOX treatment.

Western blot was utilized to measure expression of the nuclear transcription factor NRF1 (Figure 3F) and its coactivator PGC1 α (Figure 3G), because they are key initiators of the mitochondrial biogenesis pathway. Expression of these proteins was significantly elevated in the hearts of *cs*-HO-1 mice treated with DOX compared to WT controls. In addition, relative to vehicle-treated controls, PGC1 α expression was induced in *cs*-HO-1 mice but not WT mice treated with DOX. Expression of TFAM, a mitochondria-specific transcription factor

that initiates the biogenesis pathway, was only induced in *cs*-HO-1 mice treated with DOX (Figure 3H).

Global and cardiac-specific HO-1 overexpression prevent DOX-induced mitochondrial damage

To determine if the protective effects of HO-1 overexpression extended to the subcellular level and to examine the myocardium for indicators of mitochondrial dysfunction secondary to suppressed mitochondrial biogenesis in WT mice, sections of LV myocardium were evaluated by transmission electron microscopy (TEM) 14 and 60 days after treatment with DOX or vehicle. Hearts from WT mice treated with DOX exhibited marked subcellular abnormalities compared to vehicle-treated controls (Figure 4, A and B), with dilation of the sarcoplasmic reticulum (SR), (Figure 4B), especially in areas of disorganized myofibrils. Strikingly, there was an apparent increase in the overall number of mitochondria in WT mice treated with DOX (Supplemental Figure 4). However, these mitochondria were small, thus suggesting an increase in mitochondrial fragmentation in DOX-treated hearts. These features were not observed in heart tissue obtained from HBAC (Figure 4, C and D) or *cs*-HO-1 mice (Figure 4, E, F, and I) treated with DOX. Intercalated discs with deranged morphology were also frequently observed in treated WT mice but not *cs*-HO-1 mice (Figure 4, G–I).

The subcellular changes observed at day 14 were found to persist for at least 60 days after treatment, as did the apparent protection by HO-1 overexpression (Figure 5). In WT mice, there was a continued presence of fragmented mitochondria and intracellular vacuoles lacking a boundary membrane (Figure 5D and Supplemental Figure 4). Myocytes from *cs*-HO-1 mice lacked these vacuoles but contained electron-lucent circular structures bounded by a membrane (Figure 5, B and E), which is characteristic of autophagic vacuoles. These structures were present in myocytes from both DOX- and vehicle-treated *cs*-HO-1 mice. It is interesting to note that myocytes from HO-1^{-/-} mice treated with DOX contained clearly abnormal electron-lucent mitochondria, many of which appeared to be incorporated in membrane-bound vacuoles (Figure 5F).

To quantitate the effect of both HO-1 expression and DOX treatment on mitochondrial number and size, the number of mitochondria and their average area per 5 fields at $\times 1,650$ magnification was determined. There was a significant increase in the number of mitochondria in myocytes from WT mice versus myocytes from *cs*-HO-1 mice at both day 14 and 60 after treatment (Figure 5G). Despite an overall increase in the number of mitochondria per high-powered field, there was a decrease in the average size of mitochondria in WT mice treated with DOX (Figure 5H). These results suggest that, in addition to promoting mitochondrial biogenesis, HO-1 expression may also prevent DOX-induced mitochondrial fragmentation.

HO-1 overexpression regulates the mediators of mitochondrial dynamics

Mitochondrial dynamics encompass the balance between mitochondrial fission and fusion (45, 46). Oxidative stress results in the fragmentation of damaged mitochondria and subsequent clearance by mitophagy (22, 47, 48). Mitochondrial fragmentation could be the result of either decreased fusion (Mfn1 and Mfn2) or increased fission (DRP1 and Fis1)

(49). Given that TEM analysis suggested evidence of possible fission in WT mice treated with DOX, we examined expression of the mediators of both fission and fusion in the hearts of mice 14 days after treatment. DOX treatment resulted in increased expression of Mfn1, but not Mfn2, in WT mice. However, HO-1 overexpression was associated with marked upregulation of both of the fusion proteins after DOX treatment (Figure 6, A and B, and Supplemental Figure 2). There was no difference in the expression of DRP1 between the groups (Figure 6C). However, HO-1 overexpression in *cs*-HO-1 mice prevented increased expression of Fis1, a fission-related protein that has been shown to trigger mitophagy, which was observed in WT mice treated with DOX (Figure 6D and refs. 19, 50). Collectively, these data suggest that HO-1 overexpression prevents mitochondrial fragmentation by regulating mitochondrial dynamics.

HO-1 expression prevents nonhomeostatic alterations in the mitophagy pathway

Mitochondrial dynamics are intimately linked to the clearance of damaged or senescent mitochondria through mitophagy (15). Therefore, this pathway was examined as a function of time in WT mice treated with DOX and compared to untreated controls. Expression of the key mediators of mitophagy, PINK1 and parkin, initially declined after DOX treatment (Figure 7A, day 5 and 8, and Supplemental Figure 3). However, at day 14, the levels of these proteins appeared to increase substantially relative to untreated control samples (Figure 7A). Interestingly, the temporal suppression of mitophagy appears to correlate with an increase in apoptotic cell death, as suggested by an increase in caspase-3 expression at day 5 (Figure 7A).

Damaged mitochondria that undergo fission are cleared from the cell by mitophagy, which is important since dysfunctional mitochondria are potent stimuli for the induction of cell death by apoptosis (51). To test the hypothesis that HO-1 overexpression prevents DOX-induced alterations in the mitophagy pathway, *cs*-HO-1 mice were treated with DOX, and PINK1 expression in the heart was compared to its levels in untreated controls and WT mice treated with DOX (Figure 7B). *cs*-HO-1 mice expressed increased levels of PINK1 at baseline, relative to untreated WT controls, and the level of PINK1 expression remained unchanged from baseline in *cs*-HO-1 mice treated with DOX. In contrast, PINK1 expression was decreased at day 5 and increased at day 14 in WT mice, relative to untreated WT controls (Figure 7B). These data suggest that HO-1 overexpression not only leads to increased basal expression of PINK1 but also prevents dynamic changes in mitophagy progression over time that are characteristic of WT mice treated with DOX.

Discussion

In this study, we established a model of anthracycline-induced mitochondrial dysfunction in cardiac myocytes to study the *in vivo* role of HO-1 expression in mitochondrial quality control, a term collectively encompassing mitochondrial fission and fusion (i.e., dynamics), biogenesis, and mitophagy. Treatment of WT mice with 18 mg/kg of DOX over a 1-week period resulted in dilated cardiomyopathy, as determined by reduced LV EF, increased mean LV diameter in systole and diastole, and decreased LV posterior wall thickness. Concomitant with the appearance of these gross functional and architectural changes of the LV, marked

changes in myocyte subcellular morphology were also observed. The most notable of these was indications of a decline in the quality of the mitochondria, likely secondary to attendant oxidative stress. Quantitative morphometric analysis showed that mitochondria in the hearts of WT mice treated with DOX were more numerous and smaller. Other subcellular derangements included dilation of the SR and the appearance of vacuoles that appeared to lack a boundary membrane. Using mouse strains in which HO-1 is overexpressed globally or specifically within the myocardium, we showed that HO-1 protects against these changes in DOX-treated mice. In addition, membrane-bound vacuoles located in close proximity to mitochondria were more abundant in *cs*-HO-1 and HBAC mice that overexpress HO-1, independent of treatment with DOX or vehicle. Evaluation of mitochondrial molecular pathology demonstrated that this protection was at least partially mediated through preservation of the expression of proteins involved in mitochondrial biogenesis, including NRF1, its coactivator PGC1 α , and their downstream target TFAM, a mitochondrial transcription factor that signals for mtDNA replication. Decreased mtDNA and Poly expression in WT mice but not *cs*-HO-1 mice treated with DOX confirmed further impairment of mitochondrial biogenesis. Interestingly, while DOX treatment resulted in a significant elevation of NRF1 expression in WT mice treated with DOX, there was no concomitant increase in the expression of its coactivator PGC1 α , the master regulator of mitochondrial biogenesis (41, 52–54), which is reflected by static levels of TFAM in WT mice but not *cs*-HO-1 mice treated with DOX. Collectively, these findings suggest that an increased level of HO-1 in cardiomyocytes is sufficient to promote biogenesis after mitochondrial damage.

Mitochondrial dynamics are tightly regulated, and when perturbed it is difficult to surmise if the changes that occur are a cause or an effect of an underlying pathophysiology (15, 22, 25, 55–59). For example, cardiac DRP1 deficiency leads to an uncoupling of mitochondrial dynamics with the process of mitophagy and results in cardiomyocyte apoptosis, cardiac dysfunction, and mortality (58). Therefore, DRP1 expression appears to be essential in the clearance of damaged or senescent mitochondria from the heart, which is mediated by mitophagy. DRP1/mitophagy-mediated clearance of damaged mitochondria is essential, because they are potent sources of ROS. In this study, we demonstrated that, although there was no change in total DRP1 levels in WT or *cs*-HO-1 mice treated with DOX compared to WT controls, DOX treatment caused a significant increase in Fis1 expression. The upregulation of Fis1 expression after DOX treatment supports our observations made with TEM, which demonstrated evidence of mitochondrial fragmentation in WT mice treated with DOX. Importantly, it appears that HO-1 overexpression prevents mitochondrial fragmentation both on TEM evaluation and by preventing upregulated Fis1 expression. Whether HO-1 inhibits mitochondrial fragmentation in the context of oxidative stress by directly regulating the expression of Fis1 or other upstream fission proteins or by preventing mitochondrial damage that signals secondarily for upregulated fission is an important topic for future investigation. However, given that we demonstrated that the mitophagy pathway is highly active at day 14 in WT mice treated with DOX (relative to basal values), it is likely that DOX causes mitochondrial damage, thus triggering fission of damaged mitochondrial segments and subsequent induction of mitophagy for their clearance.

While the role for HO-1 in mitochondrial fission may be an indirect function of exaggerated mitochondrial injury in WT versus *cs*-HO-1 mice, these studies suggest a direct relationship between mitofusion and HO-1 expression. After DOX treatment, the level of expression of Mfn1 and Mfn2 was strikingly elevated in *cs*-HO-1 mice compared to both vehicle-treated controls and WT mice treated with DOX. This line of evidence suggests that HO-1 expression plays a direct role in mitochondrial fusion, which is likely linked to the herein demonstrated increase of mitochondrial biogenesis in *cs*-HO-1 mice treated with DOX. The individual roles of the mitofusin proteins are still largely unknown. As a family of proteins, the mitofusins regulate fusion of the outer mitochondrial membrane (56). Because they are expressed on the outer membrane and the SR is located in close cellular proximity to mitochondria to facilitate calcium exchange, the mitofusins facilitate mitochondria-to-SR tethering (60, 61). Interestingly, in TEM micrographs, we observed a striking dilation of the SR of WT mice treated with DOX. Therefore, the role of HO-1 expression in maintaining proper SR-to-mitochondrial localization and thus, intracellular calcium handling and excitation-contraction coupling should be the focus of future investigation.

At early time points (i.e., day 5), DOX appeared to inhibit the mitophagy pathway in WT mice but not *cs*-HO-1 mice treated with DOX. Autophagy and mitophagy are dynamic pathways; the flux through these pathways changes to meet the metabolic, energetic, and homeostatic demands of the cell, particularly when these processes are deranged by noxious stimuli, such as DOX or ischemia/reperfusion injury (56, 59, 62, 63). Therefore, in this study, we examined flux through the mitophagy pathway as a function of time after DOX treatment. In WT mice, we demonstrated that DOX causes dynamic changes in the mitophagy pathway with respect to time, while HO-1 overexpression prevented these injury-induced changes such that expression of the mitophagy mediator PINK1 remained stable. Interestingly, TEM analysis revealed an increased abundance of membrane-bound autophagic vacuoles in mice that overexpress HO-1 in the heart, regardless of treatment with DOX or vehicle. This finding was confirmed by a marked elevation of PINK1 expression in *cs*-HO-1 mice relative to WT controls. Our findings suggest that increased HO-1 portends increased basal mitophagy in the heart as well as a resistance to damage-induced changes in the mitophagy pathway. Collectively, these findings suggest that mitophagy is protective against noxious cardiac stimuli, likely by regulating the turnover of damaged and senescent mitochondria and their subsequent replacement through biogenesis.

The ability of HO-1 expression to act as a rheostat in the process of macroautophagy in the kidney after nephrotoxic insults from cisplatin was previously demonstrated by our laboratory (64). Mitophagy plays a protective role in numerous disease states as it clears and recycles damaged mitochondria from cells affected by tissue injury (65, 66). Therefore, it is likely that inhibition of mitophagy by DOX and prevention of this phenomenon by HO-1 overexpression at least partially explains the molecular pathology of cardiotoxicity in this model and the protective function of HO-1 expression, respectively. These findings suggest that the increased rate of mitophagy at baseline and after DOX treatment in *cs*-HO-1 mice relative to WT controls confers beneficial properties. Collectively, we have demonstrated that HO-1 overexpression prevents mitochondrial fragmentation (i.e., fission) and the dynamic upregulation of mitophagy 14 days after DOX treatment, while, at the same time, increasing mitofusion and the generation of new mitochondria through biogenesis. Thus, it

appears that HO-1 expression is a general mitoprotective response to cardiac injury. Further investigation is needed to determine the specific mechanistic underpinnings necessary for this effect.

Previous studies demonstrated that exogenous CO inhalation protects mice from DOX-induced cardiac toxicity by modulating signaling through the Akt1 pathway, which ultimately prevents mitochondrial depletion (41, 53). Here, we have shown that overexpression of a human HO-1 transgene confers broadly protective effects in mitochondrial quality control. Future studies are warranted to determine whether the protective properties of HO-1 are secondary to catabolism of prooxidant heme, which is released secondary to damage to cells and mitochondria, and/or the benefit conferred by production of biliverdin and CO or the induction of ferritin secondary to the release of iron. This consideration is particularly important because the protection offered by HO enzyme activity is more substantial than exogenous administration of any of its byproducts in isolation. It is likely that HO-1 expression plays an integral role at the level of the mitochondria by disrupting the positive feedback loop that exists between oxidant stress and mitochondrial injury, both by degrading heme and by generating its potentially cytoprotective byproducts. In this study, we demonstrated that there was no discernible difference between HBAC mice (global HO-1 overexpression) and *cs*-HO-1 mice (cardiomyocyte-restricted HO-1 overexpression) with regard to the extent of mitochondrial protection and secondary cardiac structural damage caused by DOX. This finding suggests that overexpression of HO-1 in cardiac cells is protective independent of its expression in neighboring endothelial and vascular smooth muscle cells or intracardiac mononuclear phagocytes.

The clinical significance of these findings are multifold. Chemotherapy-induced cardiac toxicity was once believed to be a problem of the past, mitigated by the development of newer, more targeted anticancer agents. However, DOX remains a mainstay of therapy in numerous common cancers, ranging from breast to hematological malignancies in children and adults. Furthermore, it is being increasingly recognized that newly developed chemotherapeutic agents, such as trastuzumab (67–70), imatinib (71, 72), and others (73–75), also cause use-limiting cardiotoxic side effects, many of which center around mitochondrial toxicity (76, 77). This problem has become so important that it was recently recognized by the formation of the International Cardioncology Society and the creation of cardiac oncologist specialties at academic medical centers across the country (78). In addition, realization of the full clinical utility of anthracyclines and newer chemotherapeutic agents is limited, because the use of these drugs is curtailed by a direct relationship between the extent of their use and the development of cardiac toxicity in cancer survivors. An important clinical question that should be the focus of future studies is if therapies based on HO-1 could be initiated in cancer survivors to prevent the development of late cardiac toxicity. Therefore, the findings described herein are important now, as the cardiotoxic effects of new chemotherapeutics are uncovered, and in the development and clinical implementation of future novel anticancer agents.

Regarding the model employed in this study, DOX was chosen because of its known toxic effects on mitochondria (41, 43, 44, 79–81), which allowed for the role of HO-1 expression on the global process of mitochondrial quality control to be tested in vivo in a reproducible

manner. An important methodological strength of this report is that it utilizes a unique model of anthracycline-induced toxicity, wherein the drug is delivered in multiple small doses and the disease is studied at subacute (day 14) and chronic (day 60) points of cardiac disease progression. This is in contrast to bolus dosing used to study the acute phase of disease (day 1–5), which limits clinical correlation, because patients treated with DOX receive the drug over the course of 3 to 6 cycles of therapy and develop dilated cardiomyopathy months to years later. Therefore, it is more likely that the model used here more closely elucidates the long-term effect of mitochondrial damage in the heart, as opposed to the acute effects of supraphysiological doses of bolus drug.

Given that oxidative stress and alterations in mitochondrial metabolism underlie many if not most forms of cardiac failure, including acute myocardial infarction (82–85), congestive heart failure (86–88), and cardiac remodeling (89–91), the findings highlighted in this study are broadly applicable and may point to HO-1 expression as a general therapeutic target for patients with cardiovascular disease arising from a multitude of etiologies. Importantly, novel pharmacological agents that affect mitochondrial quality are in the pipeline or are being used in animal studies. Here, we have shown that therapies aimed at HO-1 induction have a mitoprotective effect in addition to their well-established antiapoptotic, antiinflammatory, and cytoprotective properties. Given these findings, future studies can confirm how HO-1 expression affects mitochondrial health in the diverse array of cardiac disease states seen in patients, including infarction, pressure/volume overload, and diabetic cardiomyopathy. Using a known mitochondrial toxin (DOX) in this study was an integral first step in establishing the relationship between HO-1 expression and mitochondrial quality control.

The complex molecular pathology caused by DOX is likely secondary to the widespread deleterious effects of free radical production, which is exacerbated by dysregulated iron homeostasis (43, 92). Interestingly, the free radicals generated by DOX are strong signals for the induction of HO-1 expression as well as induction of the transcriptional mediators of mitochondrial biogenesis and mitophagy (36–39). Previous *in vitro* studies have demonstrated that DOX inhibits HO-1 expression through a Bach1 repressor-dependent mechanism (93). *In vivo*, although DOX treatment moderately induces HO-1 expression (data not shown), forced HO-1 overexpression in transgenic mice is sufficient to ameliorate DOX-induced dilated cardiomyopathy, likely by preventing mitochondrial damage and upregulating mitoprotective responses, such as mitofusin and biogenesis. Thus, HO-1 is a promising therapeutic target in humans, in which mitochondrial pathophysiology is an underlying component of disease states of the heart and other organ systems.

Methods

Animals

Male and female mice between 10 and 16 weeks of age were used in all experiments. The 3 transgenic mouse lines and the WT controls used in this study are listed in Table 1. HBAC mice are “humanized” HO-1 mice that overexpress a human HO-1 transgene on a BAC. These mice were generated by our laboratory and globally overexpress HO-1 in all tissues, including the heart, that have been examined (42). HBAC mice were crossed with HO-1^{-/-}

mice (mixed FVB/C57BL/6 background), which are globally deficient in the expression of endogenous mouse HO-1 (94, 95). Therefore, HBAC mice overexpress human HO-1 but are deficient for the mouse gene and are on a mixed FVB/C57BL/6 background. Mice with cardiac-specific HO-1 overexpression (*cs*-HO-1; C57BL/6 background) were generated by Shaw-Fang Yet and Mark A. Perrella (Harvard Medical School, Boston, Massachusetts, USA) (82) and provided for these studies by Roberto Bolli (University of Louisville, Louisville, Kentucky, USA). These mice overexpress a human HO-1 transgene downstream of the α -myosin heavy chain gene promoter, which is highly active and expressed in a cardiac-restricted manner (82, 89). The genotype of transgenic mice was determined by PCR on DNA isolated from the tail. In mice used for experiments, the genotype was confirmed by Western blots using an anti-HO-1 antibody (reactive to human and mouse) on cardiac tissue lysates generated after euthanasia. Appropriate WT controls for each strain of transgenic mice were used. WT littermates on a mixed FVB/C57BL/6 background were used as controls for HBAC and HO-1^{-/-} mice. For *cs*-HO-1 mice, WT littermates on C57BL/6 background were used.

DOX or vehicle (saline) treatment was performed intravenously with a 28G needle via the tail vein. The mice were weighed before receiving each of the 3 treatments, which were administered over the course of 1 week, such that the total cumulative dose was 18 mg of DOX per kg of body weight (Figure 1A and the Results). Body weight was recorded at 1, 5, 14, 28, and 60 days after treatment and at the time of euthanasia and was not significantly different between the different WT and transgenic strains utilized in this study.

Transthoracic echocardiography

Echocardiography was performed as described previously (89, 96). Briefly, mice were anesthetized with 1.5% isoflurane in 95% O₂ and placed in the supine position. Body temperature was maintained at 36.5°C to 37.5°C on a heated platform, and electrocardiograms and temperature were continuously monitored. Cardiac function was assessed (M-mode and 2D) with a VisualSonics VeVo 770 Imaging System (VisualSonics) equipped with a high-frequency 30-MHz probe. Data analysis was performed using VisualSonics software (VisualSonics). All parameters were measured in the parasternal long-axis view over at least 5 consecutive cardiac cycles and averaged from at least 3 measurements. These parameters include LV end-diastolic and end-systolic diameter, anterior and posterior wall thickness in systole and diastole, LV EF, and heart rate. End-diastolic volume (EDV) and end-systolic volume (ESV) were measured using the modified Simpson's method. LV systolic function was indexed by LV EF ($EF = [EDV - ESV]/EDV \times 100$).

Western immunoblotting

Protein extraction and immunoblotting were performed as previously described (96–98). Briefly, ventricular cardiac tissue was homogenized in RIPA buffer, electrophoresed on a 10% sodium dodecyl sulfate–polyacrylamide gel, and transferred onto a Hybond C Extra membrane (Amersham Biosciences). Membranes were incubated with the following anti-mouse primary antibodies: HO-1 (Enzo Life Science, ADI-SPA-894, 1:1,000), GAPDH (Millipore, MAB374, 1:5,000), DRP-1 (BD, 611112, 1:2,000) PINK1 (Abcam, ab75487,

1:100), parkin (Abcam, ab15954, 1:100), and cleaved caspase-3 (Cell Signaling, 9664, 1:1,000), followed by a HRP-conjugated secondary antibody (1:10,000; Jackson ImmunoResearch Laboratories). HRP activity was detected by chemiluminescence. Membranes were then stripped and re probed with anti-mouse GAPDH antibody and Ponceau S reagent to confirm equal loading and transfer.

Western blot analysis of proteins involved in mitochondrial biogenesis was performed as previously described (63). Briefly, 20 μ g of assayed protein samples were resolved by sodium dodecyl sulfate–polyacrylamide gel electrophoresis using gradient gels (BioRad). The separated protein was transferred to Immobilon P membranes (Millipore) and blocked with 4% nonfat dry milk in TBST (Sigma-Aldrich). Membranes were incubated overnight at 4°C with validated antibodies against mouse. The following antibodies were purchased from Santa Cruz Biotechnologies: COX3 (1:500; sc-23986), mouse ND1 (1:1,000; sc-20493), PGC1 α (1:500; sc-13067), Poly (1:1,000; sc-390634), mouse TFAM, and mouse Mfn1 and Mfn2 (1:200; sc-166644, sc-50331). β -Actin antibody (1:5,000; Sigma-Aldrich, clone AC-74) was used as protein loading control. Antibodies for NRF1 (1:1,000) and TFAM (1:1,000) were made in-house (99). After application of primary antibodies and 3 washes in Tris-buffered saline with Tween, membranes were incubated in HRP-conjugated goat anti-rabbit IgG (1:10,000; Amersham). Blots were developed with enhanced chemiluminescence, and the protein density was quantified in the mid-dynamic range relative to β -actin (BioRad ImageQuant Software). Data are expressed relative to β -actin.

Quantitative PCR for mtDNA copy number

mtDNA was isolated from heart muscle by the mtDNA Extractor Kit (Wako Chemicals). mtDNA copy number was quantified with real-time PCR on a StepOnePlus Sequence Detector System (AB Applied Biosystems). Primers were designed for cytochrome *b* (Cyt *b* [ACCCTAGTCGAATGAAT]) with ABI Probe Design software (Applied Biosystem), and amplifications were performed on 10 ng mtDNA using PCR primers (cyt *b*-s [ACCCTAGTCGAATGAAT] and cyt *b*-as [TCTGAGTTTAATCCTGT]). One copy of linearized pGEMT–cyt *b* vector (41) was used for standard mtDNA quantification. The cyt *b* probe, 5' FAM-TTCCTCCACGAAACAGGATCAAA-TAMRA 3', contained FAM (6-carboxy-fluorescein) at the 5' end as a fluorescent reporter dye and TAMRA (6-carboxy-tetramethyl-rhodamine) at the 3' end as a quencher dye selected from a highly conserved region of the mouse cyt *b* gene. Serial dilutions of 10⁵–10¹⁰ copies of standard cyt *b* plasmid were prepared for a standard curve. Samples were tested for mtDNA at 1:100 and 1:1,000 dilutions. Samples were analyzed in triplicate, with mtDNA copy number/ng DNA determined relative to the standards containing a known number of mtDNA copies per dilution.

Light microscopy

A midsagittal section of the heart was fixed in 10% neutral buffered formalin for 16 hours, stored in 70% ethanol, and embedded in paraffin. 5- μ m sections were deparaffinized in xylene solution, rehydrated, and stained with hematoxylin and eosin (H&E) or Masson's Trichrome stain by the University of Alabama at Birmingham Comparative Pathology Laboratory. Cardiac histopathology was assessed by a pathologist who was blinded to the different

groups from at least 3 mice from each group. Images were captured using a Leica DM IRB microscope (Leica Microsystems) and Image-Pro Plus software (Media Cybernetics).

Isolation of cardiac leukocytes

As previously described (96, 100), mice were anesthetized with isoflurane (1.5% in 95% O₂), and the heart was perfused with 10 ml of ice-cold saline through the LVs and right ventricles (5 ml each). The heart was explanted and washed with PBS. The atria, right ventricle, and the great vessels were removed, and the LV was minced into small pieces and digested using 1.67 Wünsch U/ml Liberase DL (Roche Diagnostics) in RPMI-1640 medium (HyClone) for 1 hour at 37°C. PEB buffer (PBS, 2 mM EDTA, 0.5% BSA) was added to disrupt calcium-dependent cell-cell complexes and to inactivate the Liberase enzyme. Disaggregation was completed by drawing the digested suspension through a 21G needle 5 times. The homogenate was passed through a 40-µm nylon filter (Fisher) to remove undigested and fibrogenous material and then centrifuged at 300 *g*. The pellet was resuspended in buffered ammonium chloride to lyse red blood cells. After washing in PBS, cells were counted and used for experiments.

Flow cytometry

Cells were incubated with anti-mouse CD16/32 for 10 minutes on ice to block non-specific binding to FCγ3 receptors. Cells were initially stained with allophycocyanin-conjugated CD45.2 (clone 104), anti-mouse MHC II biotin (clone M5/114.15.2), phycoerythrin-conjugated anti-mouse Gr-1 (Ly6G, clone RB6-8C5), and fluorescein isothiocyanate-conjugated anti-mouse CD11b (clone M1/70) for 30 minutes on ice. Cells were washed and stained with peridinin chlorophyll protein complex-conjugated anti-mouse streptavidin for an additional 30 minutes on ice. Isotype-matched, fluorochrome conjugated antibodies of irrelevant specificity were used as controls. Antibodies for flow cytometry were purchased from eBioscience. Data acquisition was performed on a FACSCalibur flow cytometer (BD Biosciences), and results were analyzed using FlowJo Software (Tree Star Inc.).

TEM

Mice were anesthetized with isoflurane (1.5% in 95% O₂), and following thoracotomy, the heart was quickly explanted and washed in ice-cold PBS. A midsagittal cardiac section was cut, and an approximately 1-mm³ section of LV in the subendocardial area was cut and immediately fixed (2.5% glutaraldehyde, 2.0% paraformaldehyde) for 2 to 4 hours. The University of Alabama at Birmingham High Resolution Shared Imaging Facility post-fixed, embedded, cut, and mounted the samples. Post-fixation was performed for 1 hour in 1% osmium. The fixed tissue was dehydrated through a series of 70% to 100% ethanol washes and embedded in 100% EBON overnight at 65°C. The embedded tissue blocks were then thin-sectioned using a diamond knife (Diatome, Electron Microscopy Sciences) at 70 to 80 nm (silver to pale gold using color interference) and placed on copper mesh grids. After drying, the sections were stained with the heavy metals uranyl acetate and lead citrate for contrast. The grids were then viewed on a Tecnai Twin 120 kv (FEI) transmission electron microscope. Digital images were acquired with an AMT CCD camera for analysis. For quantification of mitochondrial number and size, micrographs were collected at ×1,650 total magnification and analyzed with ImageJ software. Representative images are shown at

×4,400 (Figures 4 and 5) and at ×1,650 (Supplemental Figure 4). The data presented were collected from at least 3 mice per group, with analysis of at least 5 images per mouse.

Statistics

Data are presented as mean ± SEM. The 2-tailed Student's *t* test was used for comparison between 2 groups. ANOVA and the Newman-Keuls post-test were used for analyses comparing more than 2 groups. Differences were considered statistically significant at *P* < 0.05.

Study approval

All animal care and manipulations for experimentation were conducted in accordance with the *Guide for the Care and Use of Laboratory Animals* (8th ed. The National Academies Press, 2011). All animal studies were reviewed and approved by the Institutional Animal Care and Use Committee at the University of Alabama at Birmingham.

Supplementary Material

Refer to Web version on PubMed Central for supplementary material.

Acknowledgments

We appreciate the technical assistance of Daniel McFalls and Carnellia Lee. This work was supported by NIH grants R01 DK59600 (to A. Agarwal), R01 DK 083390 (to J.F. George and A. Agarwal), T32DK007545 (to R. Boddu), and P30 DK079337 (the core resource of the UAB-UCSD O'Brien Center; to A. Agarwal) and American Heart Association grant 13PRE17000013 (to T.D. Hull). We acknowledge the University of Alabama at Birmingham High Resolution Shared Imaging Facility (supported by Cancer Center Support grant P30 CA 013148) for assistance with TEM. We also acknowledge the University of Alabama at Birmingham Comparative Pathology Laboratory, directed by Trenton R. Schoeb, for assistance in preparing tissues for histopathological evaluation.

References

1. Araujo JA, Zhang M, Yin F. Heme oxygenase-1, oxidation, inflammation, and atherosclerosis. *Front Pharmacol.* 2012; 3:119. [PubMed: 22833723]
2. Wegiel B, Nemeth Z, Correa-Costa M, Bulmer AC, Otterbein LE. Heme oxygenase-1: a metabolic nike. *Antioxid Redox Signal.* 2014; 20(11):1709–1722. [PubMed: 24180257]
3. Wu ML, Ho YC, Lin CY, Yet SF. Heme oxygenase-1 in inflammation and cardiovascular disease. *Am J Cardiovasc Dis.* 2011; 1(2):150–158. [PubMed: 22254194]
4. Wu ML, Ho YC, Yet SF. A central role of heme oxygenase-1 in cardiovascular protection. *Antioxid Redox Signal.* 2011; 15(7):1835–1846. [PubMed: 21091076]
5. Hull TD, Agarwal A, George JF. The mononuclear phagocyte system in homeostasis and disease: a role for heme oxygenase-1. *Antioxid Redox Signal.* 2014; 20(11):1770–1788. [PubMed: 24147608]
6. Tenhunen R, Marver HS, Schmid R. Microsomal heme oxygenase. Characterization of the enzyme. *J Biol Chem.* 1969; 244(23):6388–6394. [PubMed: 4390967]
7. Tenhunen R, Marver HS, Schmid R. The enzymatic catabolism of hemoglobin: stimulation of microsomal heme oxygenase by hemin. *J Lab Clin Med.* 1970; 75(3):410–421. [PubMed: 4392030]
8. Tenhunen R, Marver H, Pimstone NR, Trager WF, Cooper DY, Schmid R. Enzymatic degradation of heme. Oxygenative cleavage requiring cytochrome P-450. *Biochemistry.* 1972; 11(9):1716–1720. [PubMed: 4402159]
9. Tenhunen R, Marver HS, Schmid R. The enzymatic conversion of heme to bilirubin by microsomal heme oxygenase. *Proc Natl Acad Sci U S A.* 1968; 61(2):748–755. [PubMed: 4386763]

10. Stocker R, Glazer AN, Ames BN. Antioxidant activity of albumin-bound bilirubin. *Proc Natl Acad Sci U S A*. 1987; 84(16):5918–5922. [PubMed: 3475708]
11. Stocker R, Yamamoto Y, McDonagh AF, Glazer AN, Ames BN. Bilirubin is an antioxidant of possible physiological importance. *Science*. 1987; 235(4792):1043–1046. [PubMed: 3029864]
12. Ryter SW, Tyrrell RM. The heme synthesis and degradation pathways: role in oxidant sensitivity. Heme oxygenase has both pro- and antioxidant properties. *Free Radic Biol Med*. 2000; 28(2):289–309. [PubMed: 11281297]
13. Brouard S, et al. Carbon monoxide generated by heme oxygenase 1 suppresses endothelial cell apoptosis. *J Exp Med*. 2000; 192(7):1015–1026. [PubMed: 11015442]
14. Ryter SW, Morse D, Choi AM. Carbon monoxide and bilirubin: potential therapies for pulmonary/vascular injury and disease. *Am J Respir Cell Mol Biol*. 2007; 36(2):175–182. [PubMed: 16980550]
15. Kubli DA, Gustafsson AB. Mitochondria and mitophagy: the yin and yang of cell death control. *Circ Res*. 2012; 111(9):1208–1221. [PubMed: 23065344]
16. Chen Y, Liu Y, Dorn GW 2nd. Mitochondrial fusion is essential for organelle function and cardiac homeostasis. *Circ Res*. 2011; 109(12):1327–1331. [PubMed: 22052916]
17. Smirnova E, Griparic L, Shurland DL, van der Bliek AM. Dynamin-related protein Drp1 is required for mitochondrial division in mammalian cells. *Mol Biol Cell*. 2001; 12(8):2245–2256. [PubMed: 11514614]
18. Yoon Y, Krueger EW, Oswald BJ, McNiven MA. The mitochondrial protein hFis1 regulates mitochondrial fission in mammalian cells through an interaction with the dynamin-like protein DLP1. *Mol Cell Biol*. 2003; 23(15):5409–5420. [PubMed: 12861026]
19. Gomes LC, Scorrano L. High levels of Fis1, a pro-fission mitochondrial protein, trigger autophagy. *Biochim Biophys Acta*. 2008; 1777(7-8):860–866. [PubMed: 18515060]
20. Green D, Kroemer G. The central executioners of apoptosis: caspases or mitochondria? *Trends Cell Biol*. 1998; 8(7):267–271. [PubMed: 9714597]
21. Green DR, Reed JC. Mitochondria and apoptosis. *Science*. 1998; 281(5381):1309–1312. [PubMed: 9721092]
22. Frank M, et al. Mitophagy is triggered by mild oxidative stress in a mitochondrial fission dependent manner. *Biochim Biophys Acta*. 2012; 1823(12):2297–2310. [PubMed: 22917578]
23. Frank S, et al. The role of dynamin-related protein 1, a mediator of mitochondrial fission, in apoptosis. *Dev Cell*. 2001; 1(4):515–525. [PubMed: 11703942]
24. Vives-Bauza C, et al. PINK1-dependent recruitment of Parkin to mitochondria in mitophagy. *Proc Natl Acad Sci U S A*. 2010; 107(1):378–383. [PubMed: 19966284]
25. Matsuda N, et al. PINK1 stabilized by mitochondrial depolarization recruits Parkin to damaged mitochondria and activates latent Parkin for mitophagy. *J Cell Biol*. 2010; 189(2):211–221. [PubMed: 20404107]
26. Matsuda N, Tanaka K. Uncovering the roles of PINK1 and parkin in mitophagy. *Autophagy*. 2010; 6(7):952–954. [PubMed: 20724841]
27. Geisler S, et al. PINK1/Parkin-mediated mitophagy is dependent on VDAC1 and p62/SQSTM1. *Nat Cell Biol*. 2010; 12(2):119–131. [PubMed: 20098416]
28. Geisler S, et al. The PINK1/Parkin-mediated mitophagy is compromised by PD-associated mutations. *Autophagy*. 2010; 6(7):871–878. [PubMed: 20798600]
29. Kawajiri S, et al. PINK1 is recruited to mitochondria with parkin and associates with LC3 in mitophagy. *FEBS Lett*. 2010; 584(6):1073–1079. [PubMed: 20153330]
30. Hickson-Bick DL, Jones C, Buja LM. Stimulation of mitochondrial biogenesis and autophagy by lipopolysaccharide in the neonatal rat cardiomyocyte protects against programmed cell death. *J Mol Cell Cardiol*. 2008; 44(2):411–418. [PubMed: 18062988]
31. Andersson U, Scarpulla RC. Pgc-1-related coactivator, a novel, serum-inducible coactivator of nuclear respiratory factor 1-dependent transcription in mammalian cells. *Mol Cell Biol*. 2001; 21(11):3738–3749. [PubMed: 11340167]

32. Dairaghi DJ, Shadel GS, Clayton DA. Human mitochondrial transcription factor A and promoter spacing integrity are required for transcription initiation. *Biochim Biophys Acta*. 1995; 1271(1): 127–134. [PubMed: 7599198]
33. Falkenberg M, Gaspari M, Rantanen A, Trifunovic A, Larsson NG, Gustafsson CM. Mitochondrial transcription factors B1 and B2 activate transcription of human mtDNA. *Nat Genet*. 2002; 31(3): 289–294. [PubMed: 12068295]
34. Gleyzer N, Vercauteren K, Scarpulla RC. Control of mitochondrial transcription specificity factors (TFB1M and TFB2M) by nuclear respiratory factors (NRF-1 and NRF-2) and PGC-1 family coactivators. *Mol Cell Biol*. 2005; 25(4):1354–1366. [PubMed: 15684387]
35. Kelly DP, Scarpulla RC. Transcriptional regulatory circuits controlling mitochondrial biogenesis and function. *Genes Dev*. 2004; 18(4):357–368. [PubMed: 15004004]
36. Alam J, Stewart D, Touchard C, Boinapally S, Choi AM, Cook JL. Nrf2, a Cap'n'Collar transcription factor, regulates induction of the heme oxygenase-1 gene. *J Biol Chem*. 1999; 274(37):26071–26078. [PubMed: 10473555]
37. Chang AL, Ulrich A, Suliman HB, Piantadosi CA. Redox regulation of mitophagy in the lung during murine *Staphylococcus aureus* sepsis. *Free Radic Biol Med*. 2015; 78:179–189. [PubMed: 25450328]
38. Cherry AD, Suliman HB, Bartz RR, Piantadosi CA. Peroxisome proliferator-activated receptor gamma co-activator 1-alpha as a critical co-activator of the murine hepatic oxidative stress response and mitochondrial biogenesis in *Staphylococcus aureus* sepsis. *J Biol Chem*. 2014; 289(1):41–52. [PubMed: 24253037]
39. Jalszynski P, et al. Dysfunction of Nrf2 decreases KBrO3-induced oxidative DNA damage in Ogg1-null mice. *Biochem Biophys Res Commun*. 2007; 364(4):966–971. [PubMed: 17971305]
40. Song M, Mihara K, Chen Y, Scorrano L, Dorn GW 2nd. Mitochondrial fission and fusion factors reciprocally orchestrate mitophagic culling in mouse hearts and cultured fibroblasts. *Cell Metab*. 2015; 21(2):273–285. [PubMed: 25600785]
41. Suliman HB, Carraway MS, Ali AS, Reynolds CM, Welty-Wolf KE, Piantadosi CA. The CO/HO system reverses inhibition of mitochondrial biogenesis and prevents murine doxorubicin cardiomyopathy. *J Clin Invest*. 2007; 117(12):3730–3741. [PubMed: 18037988]
42. Kim J, et al. In vivo regulation of the heme oxygenase-1 gene in humanized transgenic mice. *Kidney Int*. 2012; 82(3):278–291. [PubMed: 22495295]
43. Ichikawa Y, et al. Cardiotoxicity of doxorubicin is mediated through mitochondrial iron accumulation. *J Clin Invest*. 2014; 124(2):617–630. [PubMed: 24382354]
44. Zhang S, et al. Identification of the molecular basis of doxorubicin-induced cardiotoxicity. *Nat Med*. 2012; 18(11):1639–1642. [PubMed: 23104132]
45. Detmer SA, Chan DC. Functions and dysfunctions of mitochondrial dynamics. *Nat Rev Mol Cell Biol*. 2007; 8(11):870–879. [PubMed: 17928812]
46. Yang Y, et al. Pink1 regulates mitochondrial dynamics through interaction with the fission/fusion machinery. *Proc Natl Acad Sci U S A*. 2008; 105(19):7070–7075. [PubMed: 18443288]
47. Dagda RK, et al. Loss of PINK1 function promotes mitophagy through effects on oxidative stress and mitochondrial fission. *J Biol Chem*. 2009; 284(20):13843–13855. [PubMed: 19279012]
48. Lemasters JJ. Selective mitochondrial autophagy, or mitophagy, as a targeted defense against oxidative stress, mitochondrial dysfunction, and aging. *Rejuvenation Res*. 2005; 8(1):3–5. [PubMed: 15798367]
49. Dorn GW 2nd. Mitochondrial dynamics in heart disease. *Biochim Biophys Acta*. 2013; 1833(1): 233–241. [PubMed: 22450031]
50. Wang K, et al.
51. Kwong JQ, Molkenin JD. Physiological and pathological roles of the mitochondrial permeability transition pore in the heart. *Cell Metab*. 2015; 21(2):206–214. [PubMed: 25651175]
52. Fernandez-Marcos PJ, Auwerx J. Regulation of PGC-1alpha, a nodal regulator of mitochondrial biogenesis. *Am J Clin Nutr*. 2011; 93(4):884S–890S. [PubMed: 21289221]
53. Piantadosi CA, Carr away MS, Babiker A, Suliman HB. Heme oxygenase-1 regulates cardiac mitochondrial biogenesis via Nrf2-mediated transcriptional control of nuclear respiratory factor-1. *Circ Res*. 2008; 103(11):1232–1240. [PubMed: 18845810]

54. Ventura-Clapier R, Garnier A, Veksler V. Transcriptional control of mitochondrial biogenesis: the central role of PGC-1 α . *Cardiovasc Res*. 2008; 79(2):208–217. [PubMed: 18430751]
55. Ding WX, et al. Parkin and mitofusins reciprocally regulate mitophagy and mitochondrial spheroid formation. *J Biol Chem*. 2012; 287(50):42379–42388. [PubMed: 23095748]
56. Gegg ME, Cooper JM, Chau KY, Rojo M, Schapira AH, Taanman JW. Mitofusin 1 and mitofusin 2 are ubiquitinated in a PINK1/parkin-dependent manner upon induction of mitophagy. *Hum Mol Genet*. 2010; 19(24):4861–4870. [PubMed: 20871098]
57. Huang C, Andres AM, Ratliff EP, Hernandez G, Lee P, Gottlieb RA. Preconditioning involves selective mitophagy mediated by Parkin and p62/SQSTM1. *PLoS One*. 2011; 6(6):e20975. [PubMed: 21687634]
58. Kageyama Y, et al. Parkin-independent mitophagy requires Drp1 and maintains the integrity of mammalian heart and brain. *EMBO J*. 2014; 33(23):2798–2813. [PubMed: 25349190]
59. Shires SE, Gustafsson AB. Mitophagy and heart failure. *J Mol Med (Berl)*. 2015; 93(3):253–262. [PubMed: 25609139]
60. de Brito OM, Scorrano L. Mitofusin 2 tethers endoplasmic reticulum to mitochondria. *Nature*. 2008; 456(7222):605–610. [PubMed: 19052620]
61. Koshiba T, Detmer SA, Kaiser JT, Chen H, McCaffery JM, Chan DC. Structural basis of mitochondrial tethering by mitofusin complexes. *Science*. 2004; 305(5685):858–862. [PubMed: 15297672]
62. Gegg ME, Schapira AH. PINK1-parkin-dependent mitophagy involves ubiquitination of mitofusins 1 and 2: implications for Parkinson disease pathogenesis. *Autophagy*. 2011; 7(2):243–245. [PubMed: 21139416]
63. Hariharan N, Zhai P, Sadoshima J. Oxidative stress stimulates autophagic flux during ischemia/reperfusion. *Antioxid Redox Signal*. 2011; 14(11):2179–2190. [PubMed: 20812860]
64. Bolisetty S, et al. Heme oxygenase-1 inhibits renal tubular macroautophagy in acute kidney injury. *J Am Soc Nephrol*. 2010; 21(10):1702–1712. [PubMed: 20705711]
65. Hoshino A, et al. p53-TIGAR axis attenuates mitophagy to exacerbate cardiac damage after ischemia. *J Mol Cell Cardiol*. 2012; 52(1):175–184. [PubMed: 22044588]
66. Sciarretta S, Hariharan N, Monden Y, Zablocki D, Sadoshima J. Is autophagy in response to ischemia and reperfusion protective or detrimental for the heart? *Pediatr Cardiol*. 2011; 32(3):275–281. [PubMed: 21170742]
67. Keefe DL. Trastuzumab-associated cardiotoxicity. *Cancer*. 2002; 95(7):1592–1600. [PubMed: 12237930]
68. Patane S. Cardiotoxicity: trastuzumab and cancer survivors. *Int J Cardiol*. 2014; 177(2):554–556. [PubMed: 25205483]
69. Seidman A, et al. Cardiac dysfunction in the trastuzumab clinical trials experience. *J Clin Oncol*. 2002; 20(5):1215–1221. [PubMed: 11870163]
70. Sparano JA. Cardiac toxicity of trastuzumab (Herceptin): implications for the design of adjuvant trials. *Semin Oncol*. 2001; 28(1 suppl 3):20–27. [PubMed: 11301371]
71. Barr LA, et al. Imatinib activates pathological hypertrophy by altering myocyte calcium regulation. *Clin Transl Sci*. 2014; 7(5):360–367. [PubMed: 24931551]
72. Kerkela R, et al. Cardiotoxicity of the cancer therapeutic agent imatinib mesylate. *Nat Med*. 2006; 12(8):908–916. [PubMed: 16862153]
73. Choueiri TK, et al. Congestive heart failure risk in patients with breast cancer treated with bevacizumab. *J Clin Oncol*. 2011; 29(6):632–638. [PubMed: 21205755]
74. Duran JM, et al. Sorafenib cardiotoxicity increases mortality after myocardial infarction. *Circ Res*. 2014; 114(11):1700–1712. [PubMed: 24718482]
75. Richards CJ, et al. Incidence and risk of congestive heart failure in patients with renal and nonrenal cell carcinoma treated with sunitinib. *J Clin Oncol*. 2011; 29(25):3450–3456. [PubMed: 21810682]
76. Varga ZV, Ferdinandy P, Liaudet L, Pacher P. Drug-induced mitochondrial dysfunction and cardiotoxicity. *Am J Physiol Heart Circ Physiol*. 2015; 309(9):H1453–H1467. [PubMed: 26386112]

77. Lal H, Kolaja KL, Force T. Cancer genetics and the cardiotoxicity of the therapeutics. *J Am Coll Cardiol.* 2013; 61(3):267–274. [PubMed: 23328609]
78. Todaro MC, Oreto L, Qamar R, Paterick TE, Carerj S, Khandheria BK. Cardioncology: state of the heart. *Int J Cardiol.* 2013; 168(2):680–687. [PubMed: 23639459]
79. Kuznetsov AV, Margreiter R, Amberger A, Saks V, Grimm M. Changes in mitochondrial redox state, membrane potential and calcium precede mitochondrial dysfunction in doxorubicin-induced cell death. *Biochim Biophys Acta.* 2011; 1813(6):1144–1152. [PubMed: 21406203]
80. Octavia Y, Tocchetti CG, Gabrielson KL, Janssens S, Crijns HJ, Moens AL. Doxorubicin-induced cardiomyopathy: from molecular mechanisms to therapeutic strategies. *J Mol Cell Cardiol.* 2012; 52(6):1213–1225. [PubMed: 22465037]
81. Zhang Y, et al. Doxorubicin induces sarcoplasmic reticulum calcium regulation dysfunction via the decrease of SERCA2 and phospholamban expressions in rats. *Cell Biochem Biophys.* 2014; 70(3):1791–1798. [PubMed: 25027095]
82. Yet SF, et al. Cardiac-specific expression of heme oxygenase-1 protects against ischemia and reperfusion injury in transgenic mice. *Circ Res.* 2001; 89(2):168–173. [PubMed: 11463724]
83. Gomez L, et al. Inhibition of mitochondrial permeability transition improves functional recovery and reduces mortality following acute myocardial infarction in mice. *Am J Physiol Heart Circ Physiol.* 2007; 293(3):H1654–H1661. [PubMed: 17557911]
84. Ide T, et al. Mitochondrial DNA damage and dysfunction associated with oxidative stress in failing hearts after myocardial infarction. *Circ Res.* 2001; 88(5):529–535. [PubMed: 11249877]
85. Ikeuchi M, et al. Overexpression of mitochondrial transcription factor a ameliorates mitochondrial deficiencies and cardiac failure after myocardial infarction. *Circulation.* 2005; 112(5):683–690. [PubMed: 16043643]
86. Narula J, et al. Apoptosis in heart failure: release of cytochrome c from mitochondria and activation of caspase-3 in human cardiomyopathy. *Proc Natl Acad Sci U S A.* 1999; 96(14):8144–8149. [PubMed: 10393962]
87. Rosca MG, et al. Cardiac mitochondria in heart failure: decrease in respirasomes and oxidative phosphorylation. *Cardiovasc Res.* 2008; 80(1):30–39. [PubMed: 18710878]
88. Sorescu D, Griendling KK. Reactive oxygen species, mitochondria, and NAD(P)H oxidases in the development and progression of heart failure. *Congest Heart Fail.* 2002; 8(3):132–140. [PubMed: 12045381]
89. Wang G, et al. Cardioprotective and antiapoptotic effects of heme oxygenase-1 in the failing heart. *Circulation.* 2010; 121(17):1912–1925. [PubMed: 20404253]
90. Haudek SB, Taffet GE, Schneider MD, Mann DL. TNF provokes cardiomyocyte apoptosis and cardiac remodeling through activation of multiple cell death pathways. *J Clin Invest.* 2007; 117(9):2692–2701. [PubMed: 17694177]
91. Matsushima S, et al. Overexpression of mitochondrial peroxiredoxin-3 prevents left ventricular remodeling and failure after myocardial infarction in mice. *Circulation.* 2006; 113(14):1779–1786. [PubMed: 16585391]
92. Gammella E, Maccarinelli F, Buratti P, Recalcati S, Cairo G. The role of iron in anthracycline cardiotoxicity. *Front Pharmacol.* 2014; 5:25. [PubMed: 24616701]
93. Bernuzzi F, Recalcati S, Alberghini A, Cairo G. Reactive oxygen species-independent apoptosis in doxorubicin-treated H9c2 cardiomyocytes: role for heme oxygenase-1 down-modulation. *Chem Biol Interact.* 2009; 177(1):12–20. [PubMed: 18845130]
94. Poss KD, Tonegawa S. Reduced stress defense in heme oxygenase 1-deficient cells. *Proc Natl Acad Sci U S A.* 1997; 94(20):10925–10930. [PubMed: 9380736]
95. Poss KD, Tonegawa S. Heme oxygenase 1 is required for mammalian iron reutilization. *Proc Natl Acad Sci U S A.* 1997; 94(20):10919–10924. [PubMed: 9380735]
96. Hull TD, et al. Heme oxygenase-1 expression protects the heart from acute injury caused by inducible Cre recombinase. *Lab Invest.* 2013; 93(8):868–879. [PubMed: 23732814]
97. Suliman HB, Carraway MS, Piantadosi CA. Postlipopolysaccharide oxidative damage of mitochondrial DNA. *Am J Respir Crit Care Med.* 2003; 167(4):570–579. [PubMed: 12480607]
98. Boddu R, et al. Leucine-rich repeat kinase 2 deficiency is protective in rhabdomyolysis-induced kidney injury. *Hum Mol Genet.* 2015; 24(14):4078–4093. [PubMed: 25904107]

99. Piantadosi CA, Suliman HB. Transcriptional Regulation of SDHa flavoprotein by nuclear respiratory factor-1 prevents pseudohypoxia in aerobic cardiac cells. *J Biol Chem.* 2008; 283(16): 10967–10977. [PubMed: 18252725]
100. Hull TD, et al. Heme oxygenase-1 regulates myeloid cell trafficking in AKI. *J Am Soc Nephrol.* 2015; 26(9):2139. [PubMed: 25677389]

Author Manuscript

Author Manuscript

Author Manuscript

Author Manuscript

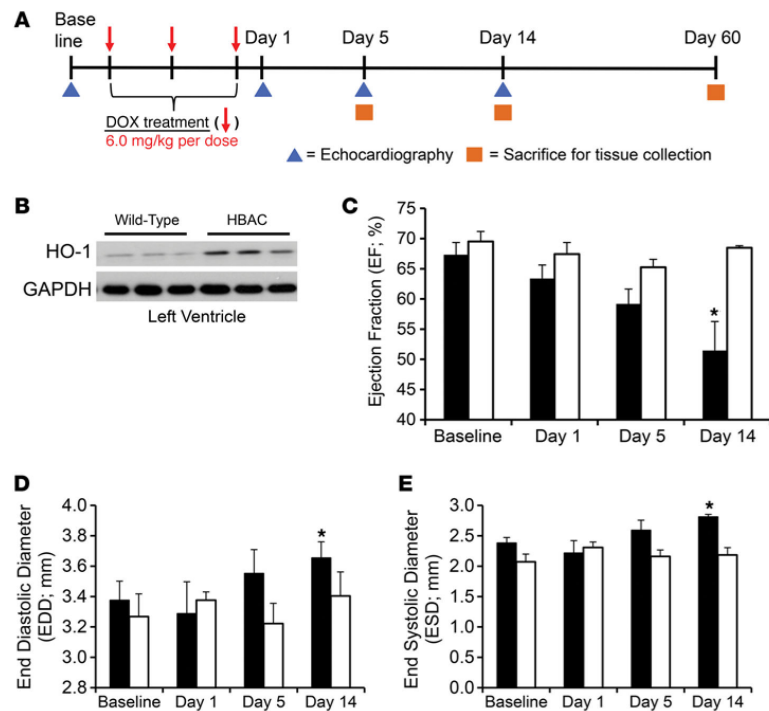


Figure 1. Heme oxygenase-1 overexpression prevents doxorubicin-induced cardiac toxicity

(A) Schematic of the treatment protocol utilized in this study. Mice were administered three 6.0 mg/kg doses of intravenous doxorubicin (DOX) every third day for a week and euthanized for tissue collection. To assess cardiac function, mice underwent serial echocardiography the day before DOX administration and up to 14 days after treatment. (B) Heme oxygenase-1 (HO-1) overexpression in humanized HO-1 overexpressing (HBAC) mice was confirmed by Western blot on tissue lysates generated from the left ventricle (LV). GAPDH was used as a loading control. (C) Ejection fraction (EF), (D) end diastolic diameter (EDD), and (E) end systolic diameter (ESD) were measured by serial echocardiography. Black bars depict data from WT mice, white bars depict data from HBAC mice. Data are presented as mean \pm SEM. * $P < 0.05$, 2-tailed paired t test was used to determine statistically significant changes after DOX treatment, relative to baseline values; $n = 5-8$ per group.

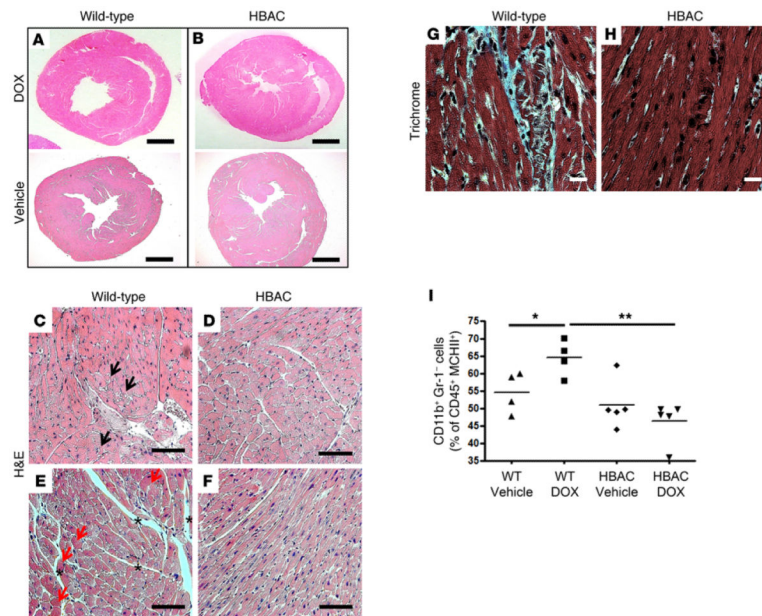


Figure 2. Heme oxygenase-1 overexpression protects cardiomyocytes from doxorubicin-mediated damage

(A and B) Representative micrographs of midsagittal sections of cardiac left ventricle (LV) from WT and humanized heme oxygenase-1 (HO-1) overexpressing (HBAC) mice 14 days after doxorubicin (DOX) treatment. Cross sections stained with H&E from (A) WT or (B) HBAC mice. Scale bar: 1 mm. (C–F) H&E-stained sections demonstrating that HO-1 overexpression prevents cardiomyocyte vacuolization (black arrows), hyper eosinophilia (red arrows), and interstitial edema (asterisks) observed in WT mice. Scale bar: 100 μ m. (G and H) Trichrome staining for fibrosis in the LV of WT and HBAC mice. Scale bar: 100 μ m. Slides were assessed by a pathologist blinded to the different groups. $n = 3–6$ per group. (I) Mononuclear phagocyte (CD45⁺CD11b⁺Gr-1⁺MHCII⁺) infiltration into the LV of WT and HBAC mice treated with DOX or vehicle was quantified by flow cytometry and expressed as a proportion of CD45⁺ cells. Horizontal bars represent mean values. * $P < 0.05$, ** $P < 0.01$, ANOVA and the Newman-Keuls post-test were used to determine statistically significant changes; $n = 3–5$ per group.

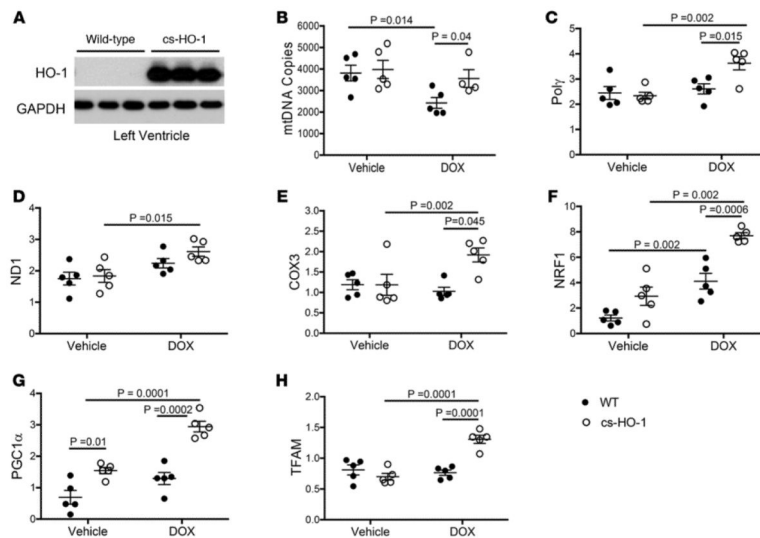


Figure 3. Heme oxygenase-1 overexpression promotes mitochondrial biogenesis

(A) Representative Western blot of heme oxygenase-1 (HO-1) expression in the left ventricle (LV) of mice with cardiac-specific overexpression of HO-1 (*cs*-HO-1). GAPDH was used as a loading control. (B) Mitochondrial DNA (mtDNA) was quantified in WT (black circles) and *cs*-HO-1 (white circles) LV obtained from mice treated with vehicle or doxorubicin (DOX) using real-time PCR. (C–E) Densitometric quantification from Western blots ($n = 5$ per group) to assess expression of the (C) mtDNA polymerase (Poly) or (D and E) components of the mitochondrial electron transport chain (NADH dehydrogenase 1 [ND1] in D and cytochrome c oxidase III [COX3] in E). (F–H) Densitometric quantification from Western blots ($n = 5$ per group) to assess expression of (F and G) nuclear (nuclear respiratory factor 1 [NRF1] and peroxisome proliferator-activated receptor γ coactivator 1 [PGC1 α]) and (H) mitochondrial (mitochondrial transcription factor A [TFAM]) transcription factors necessary for mitochondrial biogenesis. Band density was quantified relative to β -actin. Original blots can be seen in Supplemental Figure 1. Data are expressed in arbitrary units as average \pm SEM after normalization to β -actin. $P < 0.05$, ANOVA and the Newman-Keuls post-test were used to determine statistically significant changes; $n = 5$ per group.

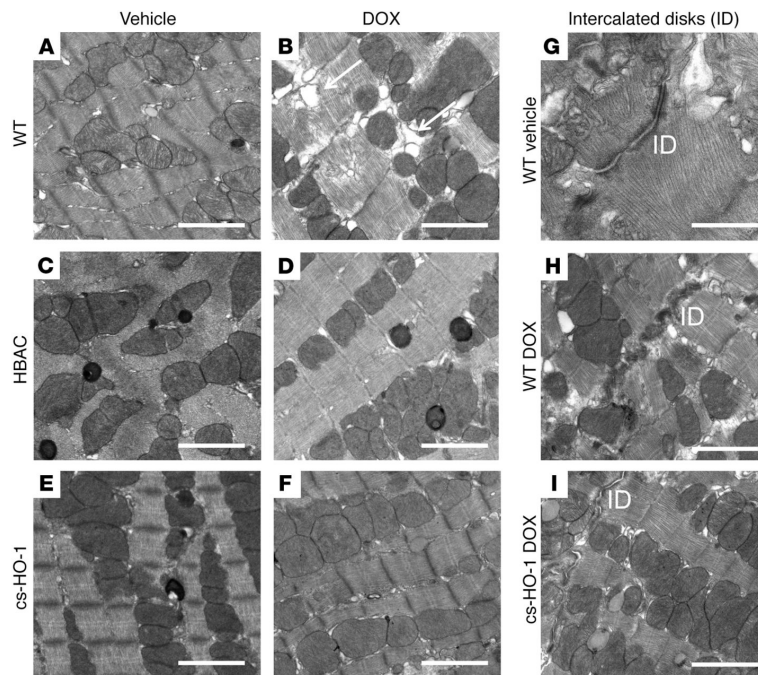


Figure 4. Doxorubicin-induced mitochondrial abnormalities at day 14

Transmission electron micrographs of the left ventricle (LV) 14 days after treatment with (A, C, and E) vehicle or (B, D, and F) doxorubicin (DOX) in (A and B) WT, (C and D) humanized heme oxygenase-1 (HO-1) overexpressing (HBAC) mice, or (E and F) mice with cardiac-specific overexpression of HO-1 (*cs*-HO-1). White arrows depict dilated sarcoplasmic reticulum. (G–I) HO-1 overexpression in *cs*-HO-1 mice prevents DOX-induced disorganization of intercalated disks (IDs). Original magnification, $\times 4,400$. Scale bar: 2 μm . $n = 3\text{--}5$ mice per group, with at least 5 images evaluated per mouse. Images were assessed by a reviewer blinded to the different groups.

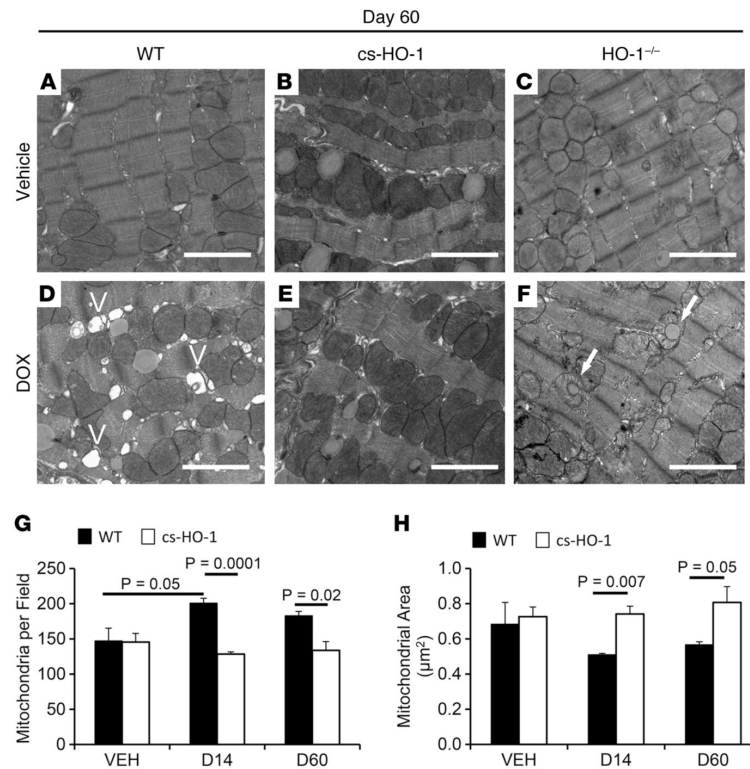


Figure 5. Doxorubicin-induced mitochondrial abnormalities at day 60

Transmission electron micrographs of the left ventricle (LV) 60 days after treatment with (A–C) vehicle or (D–F) doxorubicin (DOX) in (A and D) WT mice, (B and E) mice with cardiac-specific overexpression of heme oxygenase-1 (*cs-HO-1*), and (C and F) HO-1 knockout (*HO-1^{-/-}*) mice. White Vs mark nonmembrane-bound vacuoles, and white arrows mark mitochondria engaged with a membrane-bound vacuole. Original magnification, $\times 4,400$. Scale bar: 2 μm . (G) Mitochondrial number and (H) area were quantified on images collected at an original magnification of $\times 1,650$. Image evaluation and mitochondrial quantification were performed by a reviewer blinded to the different groups ($n = 3\text{--}5$ mice per group) and averaged from at least 5 images per mouse. Data presented as mean \pm SEM. $P < 0.05$, ANOVA and the Newman-Keuls post-test were used to determine statistically significant changes.

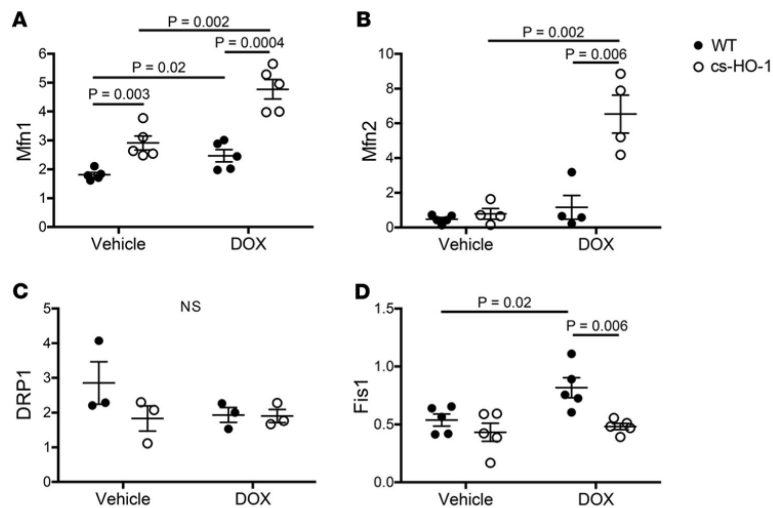


Figure 6. Heme oxygenase-1 overexpression increases fusion and inhibits fission

Expression of protein markers for mitochondrial fusion and fission was assessed in the hearts of WT mice and mice with cardiac-specific overexpression of heme oxygenase-1 (*cs*-HO-1) 14 days after treatment with vehicle or doxorubicin (DOX) by Western blot. Data are presented as protein density relative to β -actin. Black circles depict data from WT mice, and white circles depict data from *cs*-HO-1 mice. Expression of the fusion markers (A) mitofusin 1 (Mfn1) and (B) mitofusin 2 (Mfn2). Expression of the fission markers (C) dynamin-related protein 1 (DRP1) and (D) mitochondrial fission 1 (Fis1). Data are expressed in arbitrary units as an average \pm SEM after normalization to β -actin. Original blots are shown in Supplemental Figure 2. $P < 0.05$, ANOVA and the Newman-Keuls post-test used to determine statistically significant changes; $n = 5$ per group.

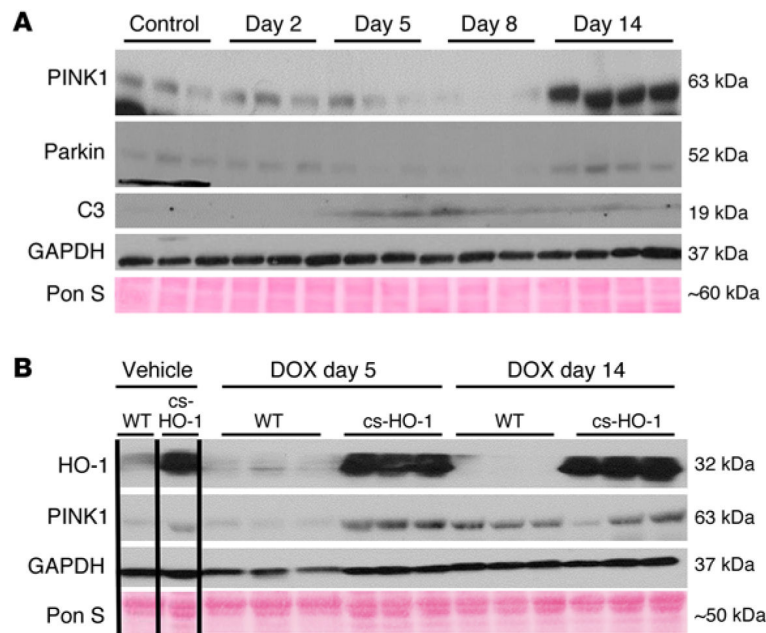


Figure 7. Heme oxygenase-1 overexpression prevents dynamic changes in mitophagy over time after mitochondrial insult

(A) WT mice were treated with doxorubicin (DOX) and euthanized 2, 5, 8, or 14 days after treatment. Levels of key protein mediators of mitophagy (PINK1 and parkin) and apoptosis (caspase-3 [C3]) were assessed by Western blot in tissue lysates prepared from the LV. GAPDH and Ponceau S (Pon S) were used as loading controls. Control mice were untreated. $n = 3-4$ per group. Densitometry plots of this blot are depicted in Supplemental Figure 3.

(B) Mitophagy was indexed by PINK1 expression in untreated WT mice and mice with cardiac-specific overexpression of heme oxygenase-1 (*cs-HO-1*) before as well as 5 and 14 days after DOX treatment. Black vertical lines indicate where the blot was cropped. All lanes in this representative image are from the same blot. GAPDH and Ponceau S were used as loading controls. $n = 3$ mice per group.

Table 1

Mouse strains used in this study

Mouse	HO-1 expression	Use
WT	WT (basal HO-1 expression)	Control strain
HBAC	Overexpression	Global HO-1 overexpression
cs-HO-1	Overexpression	Cardiomyocyte HO-1 overexpression
HO-1 ^{-/-}	Deficiency	Global HO-1 deficiency

HBAC, humanized HO-1 mice that globally/systemically overexpress a human HO-1 transgene; cs-HO-1, mice with cardiac-specific overexpression of a human HO-1 transgene driven by the α -myosin heavy chain promoter; HO-1^{-/-}; globally HO-1 deficient mice. See the Methods for additional details and strain information.

Table 2

Structural and functional parameters measured by echocardiography

	Baseline		Day 14	
	WT	HBAC	WT	HBAC
LVEDD (mm)	3.38 ± 0.13	3.27 ± 0.12	3.66 ± 0.11 ^A	3.40 ± 0.16
LVESD (mm)	2.38 ± 0.09	2.07 ± 0.10	2.84 ± 0.04 ^A	2.18 ± 0.12
LVAWTd (mm)	0.72 ± 0.03	0.80 ± 0.02	0.71 ± 0.03	0.83 ± 0.02
LVPWTd (mm)	0.70 ± 0.02	0.79 ± 0.04	0.61 ± 0.02 ^A	0.89 ± 0.06
LVAWTs (mm)	0.86 ± 0.02	0.93 ± 0.04	0.80 ± 0.03	0.98 ± 0.03
LVPWTs (mm)	1.00 ± 0.03	1.18 ± 0.06	0.82 ± 0.06 ^A	1.27 ± 0.05

Cardiac structure was measured by echocardiography before (baseline) and 14 days after DOX treatment (*n*WT mice (*n* = 5) and mice with systemic HO-1 overexpression (HBAC; *n* = 6). LVEDD, LV end-diastolic diameter; LVESD, LV end-systolic diameter; LVAWTd, anterior and posterior wall thickness in diastole; LVPWTd, LV wall thickness in diastole; LVAWTs, anterior and posterior wall thickness in systole; LVPWTs, LV wall thickness in systole. Mean ± SEM.

There were no significant differences in HBAC mice between baseline and day 14.

^A*P* < 0.05 relative to baseline.